aerospace

MDPI

Article

An Inversion Method Based on Inherent Similarity between Signals for Retrieving Source Mechanisms of Cracks

Yue Kong [1], Weimin Chen [2,3], Ning Liu [4], Boqi Kang [5] and Min Li [1,*]

[1] School of Aeronautic Science and Engineering, Beihang University, Beijing 100191, China
[2] Institute of Mechanics, Chinese Academy of Sciences, Beijing 100190, China
[3] School of Engineering Science, University of Chinese Academy of Sciences, Beijing 100049, China
[4] College of Mechanical and Electrical Engineering, Beijing University of Chemical Technology, Beijing 100029, China
[5] Key Laboratory of Space Utilization, Technology and Engineering Center for Space Utilization, Chinese Academy of Sciences, Beijing 100094, China
* Correspondence: limin@buaa.edu.cn

Abstract: The knowledge of cracking mechanisms is significant for evaluating the healthy condition of aircraft structures and can be retrieved by moment tensor inversion based on the acoustic emission (AE) phenomenon. For engineering applications, the inversion method cannot compute accurate results because the waveforms recorded by sensors are commonly contaminated by noise. Consequently, the correlation calculation of de-noising is introduced into the inversion and sufficient correlation functions are needed. In this paper, the correlation function of raw waveforms is proposed and based on the inherent similarity between the signals induced by one source and recorded by different sensors. According to the synthetic tests, the error of the inversion method based on the new correlation function is approximately 1/10 of that of the commonly used amplitude method. Although the inversion accuracy is influenced by the phase differences and the ratio of noise frequency to signal frequency, the influence is limited and the new correlation function is suitable for most practical cases. The inversion method based on the new correlation function does not require the knowledge of noise spectra or any complex calculation processes and provides a new way to improve the inversion accuracy of cracking mechanisms with little additional computation consumption.

Keywords: moment tensor; crack; acoustic emission; correlation calculation; aircraft

Citation: Kong, Y.; Chen, W.; Liu, N.; Kang, B.; Li, M. An Inversion Method Based on Inherent Similarity between Signals for Retrieving Source Mechanisms of Cracks. *Aerospace* **2022**, *9*, 654. https://doi.org/10.3390/aerospace9110654

Received: 30 August 2022
Accepted: 24 October 2022
Published: 26 October 2022

1. Introduction

For the life-safety and economic purposes of aircraft structures, some form of structural health monitoring (SHM) should be performed to evaluate the health conditions and predict the remaining fatigue life. In the SHM, the cracking mechanisms, such as cracking types and dislocation orientations, are fundamental and significant for further analysis of structural health. Cracks in aircraft structures can be inspected by various technologies, such as visual inspection, radiography [1], eddy current testing [2], and optical and ultrasonic methods [3]. However, there are still some problems when using these methods, such as requiring the aircraft to be taken out of service and being time consuming [4]. Consequently, the acoustic emission (AE) technology in the SHM has significant advantages when dealing with such problems. The AE phenomenon is that the strain energy is released rapidly when a structure undergoes crack formation and the elastic waves containing the information of cracks are stimulated. At present, AE technology has been implemented for many structures, such as wind turbine blades [5], steel bridges [6], and aircraft [7].

The commonly used AE technology can identify some general information about cracks, such as the locations, initiation, and evolution stage of cracks [8,9]. However, it cannot provide the exact mechanisms of cracks, such as source types and dislocation orientations, which are rather useful for evaluating the healthy condition of structures because

the transition between tensile and shear modes can be evident [10,11] and the propagation criteria are different for different source types [12,13]. To retrieve accurate source mechanisms of cracks, a new method of moment tensor inversion has been established. As early as 1964, Burridge and Knopoff [14] proposed the equivalent concept of a dynamic response between loads and dislocations and derived the body forces applied in the absence of a dislocation. Then, Aki and Richards [15] provided adequate derivations of the moment tensor formulas and established the inversion framework for source mechanisms. Based on Green's function, moment tensors can be calculated by the amplitude method [16,17], then source types can be classified by the decomposition of moment tensors and dislocation orientations can be calculated by the eigenvectors of moment tensors [18].

For the moment tensor inversion, the contamination of noise can hardly be avoided [19], and the inversion results are inaccurate. To improve inversion accuracy, a channel selection approach [20–22] can be implemented, where the waveforms with insufficient signal-to-noise ratios (SNRs) are discarded to directly reduce the effect of noise on inversion accuracy. The channel selection approach is efficient, but a large number of sensors are needed for data recording. Except for this approach, the Fourier transform is commonly used for de-noising, and noise can be filtered out from waveforms based on the characteristics of spectra [23–25]. This method requires information about noise and signal spectra, but the time-frequency analysis for noise spectra is quite difficult. Generally, although the above-mentioned commonly used methods are effective for improving the inversion accuracy of moment tensors, some complex calculation or analysis approaches are needed and are computationally demanding. To simplify the calculation and improve the accuracy of results, a simplified method of correlation calculation is introduced to the moment tensor inversion [26]. In this method, wave amplitudes are replaced by the correlation coefficients, which are calculated by the correlation calculation between waveforms and correlation functions. The correlation coefficients are independent of noise, thus the inversion results calculated by the correlation coefficients are accurate. Although this method is simpler than the Fourier transform, the self-defined correlation function provided by Kong, et al. [26] still requires time-frequency analysis. Consequently, to further simplify the data processing, a more concise correlation function than the self-defined correlation function is needed.

In this article, we introduced the new correlation function of raw waveforms into the correlation calculation of the moment tensor inversion. The inversion method of the new correlation function can work efficiently to improve the inversion accuracy of source mechanisms without knowledge of noise and signal spectra. This idea is based on the inherent similarity between signals induced by one source and recorded by different sensors, and no complex mathematical calculation approaches are needed. The rest of the paper is organized as follows: In Section 2, the standard moment tensor inversion is briefly reviewed, and the inversion method of the new correlation function is proposed. In Section 3, synthetic tests are carried out to verify the efficiency of the new correlation function. The effect of the two factors on the performance of the new correlation function is discussed in Section 4, and the conclusions are given in Section 5.

2. Formulas

2.1. Review of Standard Moment Tensor Inversion

Based on the moment tensor theory, a crack can be converted to a group of force couples acting at the position of the source, and the force couples can be mathematically integrated into a tensor, which is called the moment tensor. In isotropic and homogeneous media, the moment tensor components can be expressed as follows [15]:

$$M_{pq} = \left(\lambda l_k n_k \delta_{pq} + \mu l_p n_q + \mu l_q n_p\right) S_{\mathrm{f}} \tag{1}$$

where p = 1, 2, 3 and q = 1, 2, 3 represent X, Y, and Z directions, λ and μ are the Lame constants, δ_{pq} is 1m while $p = q$, otherwise it is 0. l_q represents the components of the slip vector at crack surfaces, and n_p represents the components of the normal vector to crack surfaces. S_{f} is the crack size. Moment tensors are symmetric, and 6 of the 9 components are

independent of each other. According to Equation (1), each crack has a unique moment tensor, thus the mechanism of a cracking source can be extracted from the moment tensor.

The moment tensor of a cracking source can be retrieved by AE waves, which can be explicitly expressed in terms of moment tensors. For engineering applications, compressional waves (P wave) are commonly used for the inversion, because P wave velocity is higher than shear wave (S wave) velocity. Then, the first-arrival waves are pure P waves and the inversion formulas can be simplified. According to the point-source and far-field approximations [27], the P waves generated by a fracturing source can be expressed as:

$$u_k(t) = \frac{1}{4\pi\rho\alpha^3}\frac{r_k}{R}\begin{pmatrix} r_1 & r_2 & r_3 \end{pmatrix}\begin{bmatrix} M_{11} & M_{12} & M_{13} \\ M_{12} & M_{22} & M_{23} \\ M_{13} & M_{23} & M_{33} \end{bmatrix}\begin{pmatrix} r_1 \\ r_2 \\ r_3 \end{pmatrix}\dot{S}\left(t - \frac{R}{\alpha}\right) \tag{2}$$

where $u_k(t)$ is the displacement in the kth direction (k = 1, 2, 3), r_1, r_2, and r_3 are the direction cosines from the source to the sensor. t is the time. ρ is the density of media and α is the P wave velocity. R is the source-sensor distance. $S(t)$ is the source-time function, which describes the time-dependent opening state of crack surfaces. It should be noted that the inversion equation of Equation (2) is only suitable for isotropic metallic materials. In the cases of composite or hybrid materials, wave velocities can be varied, and the inversion equation cannot be applied to those materials.

According to the amplitude inversion approach, source-time functions are commonly assumed as step functions, and the time dependence of the moment tensor inversion is ignored. Then, the inversion formula for moment tensors can be further simplified as [28]:

$$u_k = C_s\frac{r_k}{R}\begin{pmatrix} r_1 & r_2 & r_3 \end{pmatrix}\begin{bmatrix} M_{11} & M_{12} & M_{13} \\ M_{12} & M_{22} & M_{23} \\ M_{13} & M_{23} & M_{33} \end{bmatrix}\begin{pmatrix} r_1 \\ r_2 \\ r_3 \end{pmatrix} \tag{3}$$

where u_k is the amplitude of the first motion, which is the slice of the signal between the time to leave the balance position for the first time and return to the balance position again. C_s is the calibration coefficient of sensor sensitivity and material constants. According to Equation (3), although the wave velocity is involved in Equation (2), the velocity is not required in the practical cases of the moment tensor inversion. For engineering applications, the velocity and other constants are integrated into the calibration coefficient C_s, which can be obtained by the pencil-lead break experiment [28].

For one sensor, Equation (2) containing the 6 unknown moment tensor components can be obtained. Six independent components require at least 6 sensors in the inversion for one source. The linear algorithm of m ($m \geq 6$) sensors used to solve the unknown moment tensor components can be expressed in matrix form as:

$$\begin{bmatrix} G_{11} & G_{12} & G_{13} & G_{14} & G_{15} & G_{16} \\ G_{21} & G_{22} & G_{23} & G_{24} & G_{25} & G_{26} \\ \vdots & \vdots & \vdots & \vdots & \vdots & \vdots \\ G_{m1} & G_{m2} & G_{m3} & G_{m4} & G_{m5} & G_{m6} \end{bmatrix}\begin{pmatrix} M_{11} \\ M_{12} \\ M_{13} \\ M_{22} \\ M_{23} \\ M_{33} \end{pmatrix} = \begin{pmatrix} u_1 \\ u_2 \\ \vdots \\ u_m \end{pmatrix} \tag{4}$$

where G_{ij}(i = 1,2, . . . , m; j = 1, 2, . . . , 6) can be calculated by Equation (3). u_1, u_2, . . . , u_m are the amplitudes of first motions recorded by different sensors. For simplicity, Equation (4) can be rewritten as Equation (5).

$$\mathbf{G}\mathbf{M}_c = \mathbf{u} \tag{5}$$

where $\mathbf{u}$ is the column vector containing the measured wave amplitudes. $\mathbf{G}$ is the dynamic response matrix and is determined by the relative positions between sources and sensors. $\mathbf{M}_c$ contains the unknown moment tensor components in the form of a column vector.

Based on Equation (5), the moment tensors of cracking sources can be retrieved by recorded signals, and the source mechanisms can then be extracted by the decomposition of moment tensors into three basic components, which are usually isotropic (ISO), double-couple (DC), and the compensated linear vector dipole (CLVD) [18]. According to the decomposition theory [18], a retrieved moment tensor can be written as an orthonormal form as follows:

$$\mathbf{M}_{\mathrm{t}} = \begin{bmatrix} M_1 & 0 & 0 \\ 0 & M_2 & 0 \\ 0 & 0 & M_3 \end{bmatrix} \tag{6}$$

where $M_1 \geq M_2 \geq M_3$ are the eigenvalues of $\mathbf{M}$. Then the moment tensor $\mathbf{M}_{\mathrm{t}}$ can be written as a linear combination of the three basic components:

$$\mathbf{M} = M_{\mathrm{ISO}}\mathbf{E}_{\mathrm{ISO}} + M_{\mathrm{DC}}\mathbf{E}_{\mathrm{DC}} + M_{\mathrm{CLVD}}\mathbf{E}_{\mathrm{CLVD}} \tag{7}$$

where $\mathbf{E}_{\mathrm{ISO}}$, $\mathbf{E}_{\mathrm{DC}}$, and $\mathbf{E}_{\mathrm{CLVD}}$ are the ISO, DC, and CLVD elementary tensors. Then the relative scale factors C_{ISO}, C_{DC}, and C_{CLVD} are defined as:

$$\begin{bmatrix} C_{\mathrm{ISO}} \\ C_{\mathrm{DC}} \\ C_{\mathrm{CLVD}} \end{bmatrix} = \frac{1}{M} \begin{bmatrix} M_{\mathrm{ISO}} \\ M_{\mathrm{DC}} \\ M_{\mathrm{CLVD}} \end{bmatrix} \tag{8}$$

where $M = |M_{\mathrm{ISO}}| + |M_{\mathrm{DC}}| + |M_{\mathrm{CLVD}}|$. The source types can be determined by the proportions of the three components in moment tensors and illustrated by the source-type plots.

2.2. Correlation Function of Raw Waveform

For the moment tensor inversion, as the waveforms recorded by sensors are always contaminated by noise and the accurate amplitudes of first motions cannot be picked, the retrieved moment tensors are inaccurate. To solve this question, some time-frequency analysis methods can be used, and the signals of specific frequency spectra can be extracted from contaminated waveforms. According to Kong, et al. [26], for the time-frequency analysis used in the moment tensor inversion, the inversion transformation is not needed to reconstruct signals, and the correlation coefficients defined by Equation (9) can directly replace wave amplitudes to invert moment tensors.

$$\begin{aligned} a &= \mathrm{C}(\tau, u, f_{\mathrm{c}}) \\ &= \sum_{i=1}^{n} u(t_i) f_{\mathrm{c}}(t_i - \tau) \end{aligned} \tag{9}$$

where a is the correlation coefficient. C is the correlation operator. $u(t_i)$ is the waveform recorded by sensors and $f_{\mathrm{c}}(t_i)$ is the correlation function. t_i is the time. τ is the time delay between the first motions of waveforms and correlation functions.

According to the correlation coefficient defined by Equation (9), the inversion equation for moment tensors can be rewritten as follows:

$$\mathbf{G}\mathbf{M}_{\mathrm{c}}^{*} = \mathbf{a} \tag{10}$$

where $\mathbf{a}$ is the column vector of correlation coefficients a, and $\mathbf{G}$ is the dynamic response matrix in Equation (5). Importantly, in the moment tensor inversion for a specific source, the correlation function is the same for all the correlation coefficients in vector $\mathbf{a}$.

Moment tensors can be inverted in the frequency domain and noise can be filtered by the Fourier transform (FT). For the FT, the correlation function of trigonometric functions is used for de-noising. The correlation functions can also be defined manually and a self-defined correlation function is provided by Kong, et al. [26]. This self-defined function can simplify the inversion process, but the inversion accuracy is the same as that of the FT. In addition, the parameters of the self-defined function should be carefully selected.

In this study, it is proposed that the raw waveforms recorded by sensors can also be used as correlation functions to further improve the inversion accuracy. The new correlation function of raw waveforms does not require the time-frequency analysis of waveforms and no parameters need to be selected. Moreover, the inversion accuracy of the new correlation function is much better than those of the commonly used inversion methods, which can be proven by the synthetic tests in Section 3.

For comparison, the correlation function of trigonometric functions for the FT, the self-defined correlation function in Kong, et al. [26], and the correlation function of raw waveforms in this study are plotted in Figure 1.

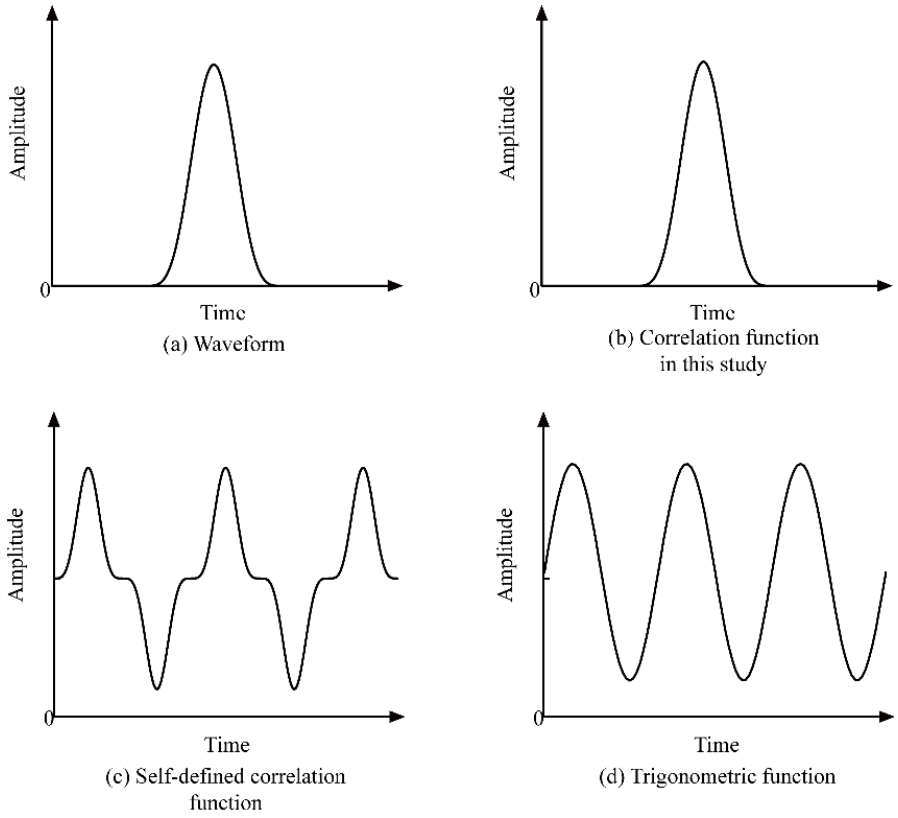

Figure 1. Comparison of correlation functions: (**a**) Simulated waveform; (**b**) raw waveform as correlation function in this study; (**c**) self-defined correlation function proposed by Kong, et al. [26]; (**d**) trigonometric function for FT.

The mechanism of the correlation function of raw waveforms for de-noising is explained in Section 2.3.

2.3. Mechanism of New Correlation Function for De-Noising

Generally, the waveforms recorded by two sensors can be expressed as follows:

$$\begin{cases} u_1(t) = u_s^1(t) + u_n^1(t) \\ u_2(t) = u_s^2(t) + u_n^2(t) \end{cases} \tag{11}$$

where $u_1(t)$ and $u_2(t)$ are the recorded waveforms, $u_s^1(t)$ and $u_s^2(t)$ are the signals, and $u_n^1(t)$ and $u_n^2(t)$ are the noise. It is logical that noise levels are different for different sensors, and the recorded waveform with an optimal signal-to-noise ratio can be chosen and regarded as the correlation function. In Equation (11), it is assumed that $u_2(t)$ is the waveform with the optimal signal-to-noise ratio and $u_n^2(t)$ can be ignored. Then $u_2(t)$ is regarded as the correlation function. The two waveforms can be rewritten as:

$$\begin{cases} u_1(t) = u_s^1(t) + u_n^1(t) \\ f_c(t) = u_2(t) = u_s^2(t) \end{cases} \tag{12}$$

For comparison, the two waveforms are plotted in Figure 2.

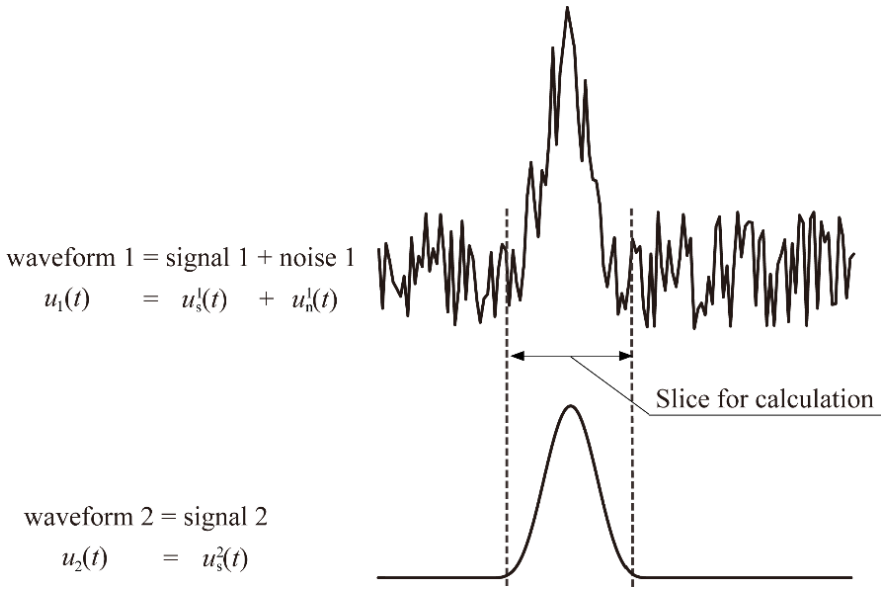

Figure 2. Comparison between the two waveforms recorded by two sensors. Waveform 2 with the optimal signal-to-noise ratio is regarded as the correlation function.

The correlation coefficient can be calculated by waveform 1 and the correlation function (waveform 2) according to Equation (9) as:

$$\begin{aligned} a &= \mathrm{C}(\tau, u_1(t), f_c(t)) \\ &= \mathrm{C}(\tau, u_s^1(t), u_s^2(t)) + \mathrm{C}(\tau, u_n^1(t), u_s^2(t)) \end{aligned} \tag{13}$$

To reduce computation consumption, we can only pick the effective waveform slice for the correlation calculation. The effective waveform slice is the slice containing signals (as shown in Figure 2).

According to Equation (2), the spectra of AE waves are dependent on the source-time function $S(t)$, and the other parameters (e.g., sensor locations and media) only affect the amplitudes of signals. For one source of the unique source-time function, the spectra of the signals recorded by different sensors are the same and the amplitudes are different for different sensors (as shown in Figure 3).

Obviously, $\mathrm{C}(\tau, u_n^1(t), u_s^2(t))$ is dependent on the signal-to-noise ratio (SNR). For a high SNR, $u_n^1(t)$ is relatively small and $\mathrm{C}(\tau, u_n^1(t), u_s^2(t))$ can also be very small. For a low SNR, $\mathrm{C}(\tau, u_n^1(t), u_s^2(t))$ can also be ignored. Besides SNR, $\mathrm{C}(\tau, u_n^1(t), u_s^2(t))$ is also dependent on the spectrum difference between signals and noise. For engineering applications, noise can be generated by various factors, and its frequency spectrum is significantly different from signals, which means the correlation between signals and noise is very small. Then, $\mathrm{C}(\tau, u_n^1(t), u_s^2(t))$ in Equation (13) is relatively small and can be ignored. The above analysis can be proven by the synthetic results in Section 4.2, when the spectrum of noise is different from that of signals. In this circumstance, the correlation coefficient of Equation (13) can be simplified as:

$$\begin{aligned} a &= \mathrm{C}(\tau, u_1(t), u_2(t)) \\ &\approx \mathrm{C}(\tau, u_s^1(t), u_s^2(t)) \end{aligned} \tag{14}$$

As shown in Equation (14), the correlation coefficient is dependent on signals and almost unaffected by noise, and the moment tensors inverted by the correlation coefficient

a are not affected by noise. Furthermore, the calculation process of Equations (13) and (14) does not require the knowledge of noise spectra, which is the advantage of the new correlation function.

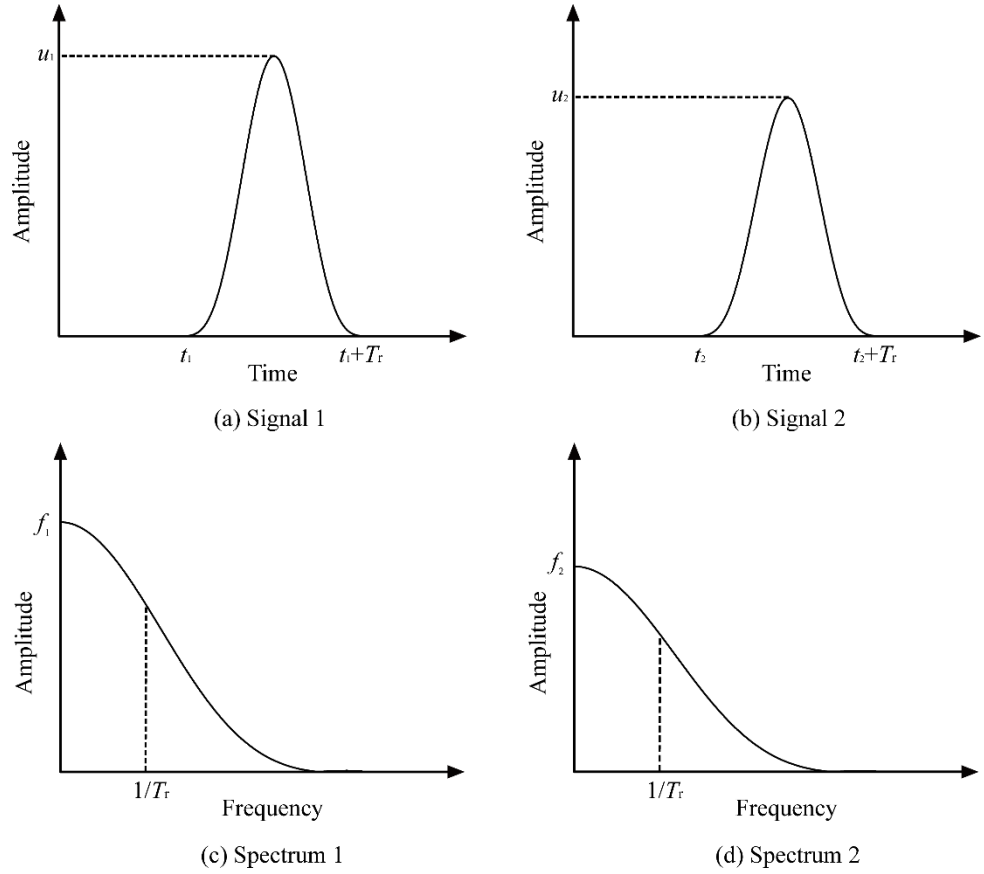

Figure 3. Two signals and corresponding frequency spectra.

If the correlation function of $f_c(t)$ is replaced by trigonometric functions or some other functions, the value of $C(\tau, u_s^1(t), f_c(t))$ decreases because of the difference in frequency spectra between the singles and correlation functions. Then, the performance of de-noising decreases and the inversion error increases.

Obviously, $\mathbf{M}_c^*$ in Equation (10) is different from $\mathbf{M}_c$ in Equation (5), but $\mathbf{M}_c^*$ can still be used for interpreting source mechanisms. Compared with the standard inversion equation of Equation (5), the inversion equation of Equation (10) based on the new correlation coefficients can be rewritten as Equation (15), because the correlation function is the same for all correlation coefficients in the inversion for one source.

$$\mathbf{G}\mathbf{M}_c^* = \beta\mathbf{u} \tag{15}$$

where β is a constant for specific inversion.

Obviously, the moment tensor solution $\mathbf{M}_c^*$ calculated by Equation (15) is different from $\mathbf{M}_c$ calculated by Equation (5). The values of $\mathbf{M}_c^*$ are inaccurate, but the relative magnitudes between the components of $\mathbf{M}_c^*$ are the same as those of $\mathbf{M}_c$. The relationship of $\mathbf{M}_c^* = \beta\mathbf{M}_c$ can be obtained. For interpreting source mechanisms, the retrieved moment tensors are decomposed into three basic tensors and the source types are identified by the proportions of the three tensors (as shown in Equations (7) and (8)). Specifically, the source types are determined by the relative magnitudes between moment tensor components. Consequently, the source types interpreted by the decomposition of $\mathbf{M}_c^*$ are the same as those of $\mathbf{M}_c$, which can also be proven by the synthetic tests in Section 3.

3. Synthetic Tests

To evaluate the performance of the inversion method based on the new correlation function of raw waveforms, synthetic tests were carried out. The AE signals are calculated by the finite element method (FEM) and the distortion of complex factors on recorded signals is represented by random white noise. Moment tensors can be calculated by distorted waveforms. The inversion errors are quantitatively illustrated by the errors of double-couple (DC) proportions and source-type plots, which are calculated by the decomposition of moment tensors according to Equations (6)–(8).

For synthetic tests, a numerical model of a thin plate is established, because thin plates are commonly used in aircraft structures. Cracks penetrate the plate thickness. Then, the moment tensor inversion can be further simplified according to Kong, et al. [29]:

$$\mathbf{M} = \begin{bmatrix} M_{11} & M_{12} & 0 \\ M_{12} & M_{22} & 0 \\ 0 & 0 & 0 \end{bmatrix} \tag{16}$$

where only three unknown moment-tensor elements need to be solved and at least three one-channel sensors are required by the inversion for one source. The inversion equation and decomposition of moment tensors in thin plates have been expressed in detail.

In the moment tensor inversion for any cracks, multiple sensors are required to record signals, and then the inversion based on the new correlation function of raw waveforms can always be achievable. In addition, the performance of the new inversion methodology is independent of sensor arrays, source types, or model shapes, because those factors are not involved in the theoretical analysis of the new methodology (Equations (9)–(15)). Consequently, a penetrated crack in a thin plate with an array of four sensors is sufficient for validating the performance of the new methodology.

3.1. Model Parameters

The plate is aluminum alloy. The material parameters are selected according to the data in references [30–32] and are listed in Table 1. The length of plate L is 2 m (as shown in Figure 4) and the thickness is 0.01 m.

Table 1. Material parameters.

Parameter	Elastic Module	Poisson's Ratio	Density
Value	7.2×10^{10} Pa	0.3	2780 kg/m^3

In the synthetic tests, four sensors are arranged as shown in Figure 4. An AE source (a crack of the length of 0.01 m) is located at the center of the plate, and the source–sensor distance R is 0.7 m.

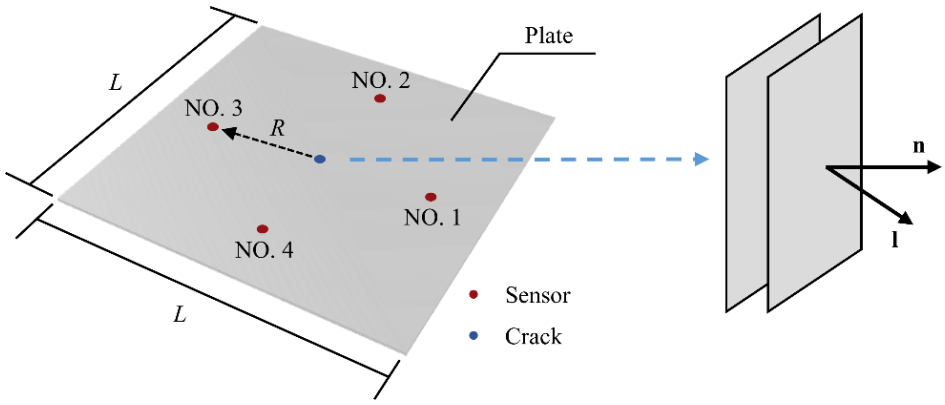

Figure 4. Sensor configuration and source (crack) location.

To stimulate the cracking process and calculate the AE signals, the AE source of precast cracks is used and its reliability has been proven [29]. For the precast crack in the FE model, the dislocation of crack surfaces is simulated by enforced displacement. Although the enforced displacement of crack surfaces is different from the true mechanism of the dislocation of crack surfaces, the stimulated AE waves are the same because the AE waves are dependent on the displacement of crack surfaces [15]. As long as the displacement of crack surfaces is the same, the stimulated AE waves are the same. In the synthetic tests, the calibration coefficient C_s is calculated by the precast crack of unit-enforced displacement.

To quantify the enforced displacement of the crack surfaces, a representative source-time function is expressed according to Ohtsu [33] as follows:

$$S(t) = \begin{cases} \frac{t}{T_r} - \frac{2}{3\pi}\sin\left(\frac{2\pi t}{T_r}\right) + \frac{1}{12\pi}\sin\left(\frac{4\pi t}{T_r}\right) & t < T_r \\ 1 & t \geq T_r \end{cases} \quad (17)$$

where T_r is the rise time. In the synthetic tests, the value of T_r is 5.0×10^{-5} s, which is based on the data in the reference [34]. It has been proven that the waveforms calculated by Equation (17) are in good agreement with those recorded in the practical experiments.

For the FE analysis, the model is meshed by hexahedron elements. For the reliability of the FE model, the time step is required to be less than the time taken for the wave to pass through an element [35]. The time step is 2.0×10^{-7} s and the shortest time for P waves to pass through an element is approximately 1.7×10^{-6} s. In addition, to suppress the effect of numerical dispersion caused by spatial discretization, 11 elements are contained within one wavelength. It should be noted that the wavelength in this study is calculated by $T_r \times \alpha$, which is different from the common concept. For AE signals, the spectrum of the waves is wide and the period is replaced by the rise time of the source-time function for simplicity.

Generally, the inversion accuracy is affected by various factors, such as an inaccurate velocity model, source location, measurement error, etc. Obviously, the study of those factors is complex. For simplicity, the effect of those factors is commonly represented by random white noise [27,36,37]. Thus, in the synthetic tests, the numerical model is kept as simple as possible and the influence of complex factors is represented by the random white noise with a uniform distribution. The noise is superimposed on the AE signals calculated by the FEM.

The pure tensile and shear source types are used in the synthetic tests, because any cracks can be the combination of those two source types. The noise levels are defined as the ratios between the amplitudes of noise and signals, and the ratios used in the tests are 0%, 10%, 20%, and 30%. The waveforms recorded by sensors No. 1, 2, and 3 are contaminated by random white noise and the waveform recorded by sensor No. 4 is pure. Then the waveform recorded by sensor No.4 is regarded as the correlation function.

The inversion errors are quantitatively represented by the DC proportions of the retrieved moment tensors, because the DC proportion is of great interest for engineering applications. The inversion errors of the solutions calculated by the amplitude and frequency methods are also provided for comparison. For the frequency method, the dominant frequency components of waveforms are used for the inversion. According to Kong, et al. [26], the inversion accuracy of the correlation-based method of self-defined correlation functions is similar to that of the frequency method. In this study, only the inversion results of the frequency method are provided. For each noise level, 100 inversions are repeated to avoid accidental errors. The average values and standard deviations of the 100 DC proportion errors are plotted to quantitatively illustrate the inversion accuracy. The source-type plots of the 10 randomly selected inversions among the 100 repeated results are provided for comparison. The source-type plot used for illustration was introduced by Vavryčuk [18].

3.2. Inversion Results

For pure tensile cracks, the inversion results calculated by the three methods are plotted in Figure 5 and the source-type plots are provided in Figure 6. The error of DC proportions in Figure 5 is the difference between the inversion and true values. In Figure 6, the source types are determined by the locations of the symbols, and the symbols of different shapes represent four noise levels. For simplicity, the inversion method based on the new correlation function of raw waveforms is denoted as the autocorrelation method.

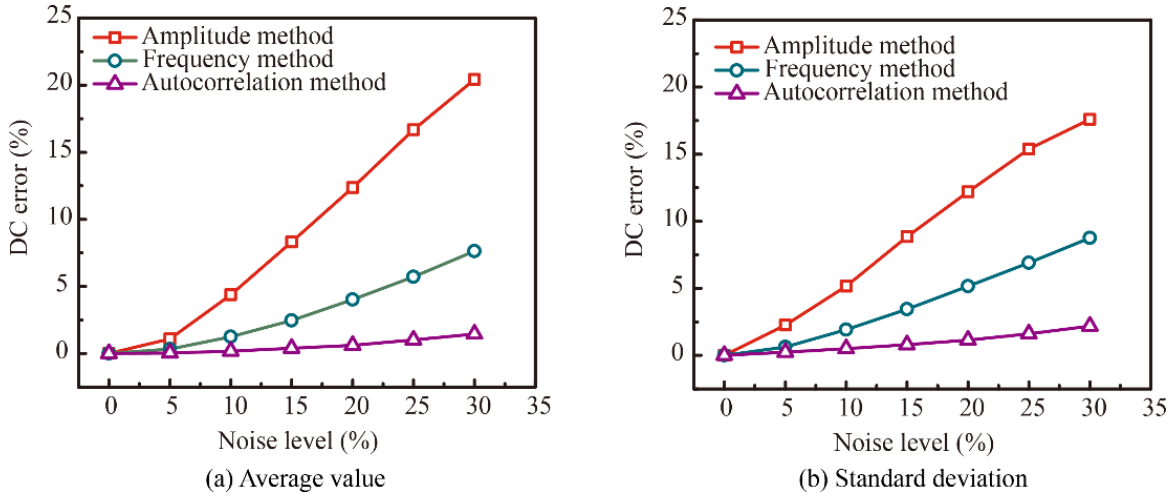

Figure 5. For pure tensile cracks, the inversion errors for different noise levels. Line types represent the results of the three inversion methods: Amplitude, frequency, and autocorrelation methods. The autocorrelation method represents the inversion method based on the new correlation function of raw waveforms for simplicity.

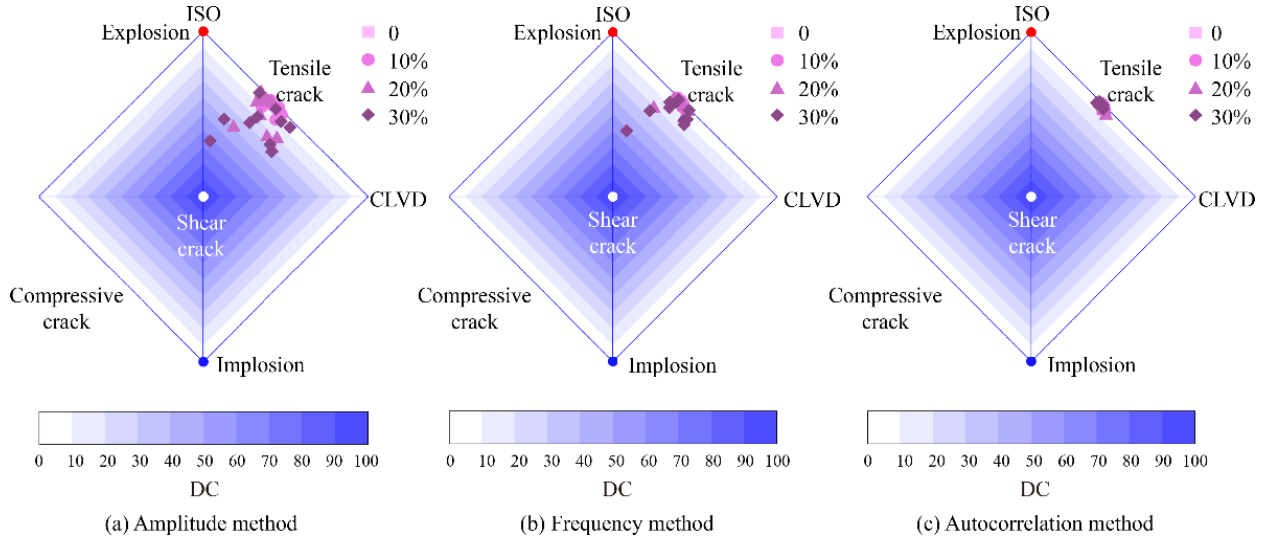

Figure 6. The source-type plots of the inversion results for the three methods for pure tensile cracks. The symbols of different shapes represent the results of different noise levels. The locations of symbols are determined by the proportions of three basic tensors (ISO, DC and CLVD) and the proportions are calculated by the decomposition of moment tensors.

As shown in Figure 5, for a noise level of 0, the errors of the retrieved DC proportions calculated by the three methods are all 0, which indicates that all three inversion methods are suitable in cases of no noise. As the noise level increases, the errors of the inversion results increase for the three methods. However, the average values of the repeated inversion

errors calculated by the autocorrelation method are more accurate than those calculated by the frequency and amplitude methods. The inversion errors of the autocorrelation method are reduced by 80% compared with the frequency method. Compared with the amplitude method, the errors of the autocorrelation method are reduced by more than 90%. The standard deviation, which indicates the stability of the repeated inversion results, also visibly improves. The standard deviation of the results calculated by the autocorrelation method is the smallest. The same phenomenon can also be observed in Figure 6, in which the symbols of the inversion results calculated by the autocorrelation method are more concentrated and closer to the true position, which indicates that the results of the autocorrelation method are more accurate and stable than those of the other two methods.

Similar conclusions can also be drawn in the inversion for shear cracks, and the inversion errors of DC proportions and the corresponding source-type plots are plotted in Figures 7 and 8, respectively.

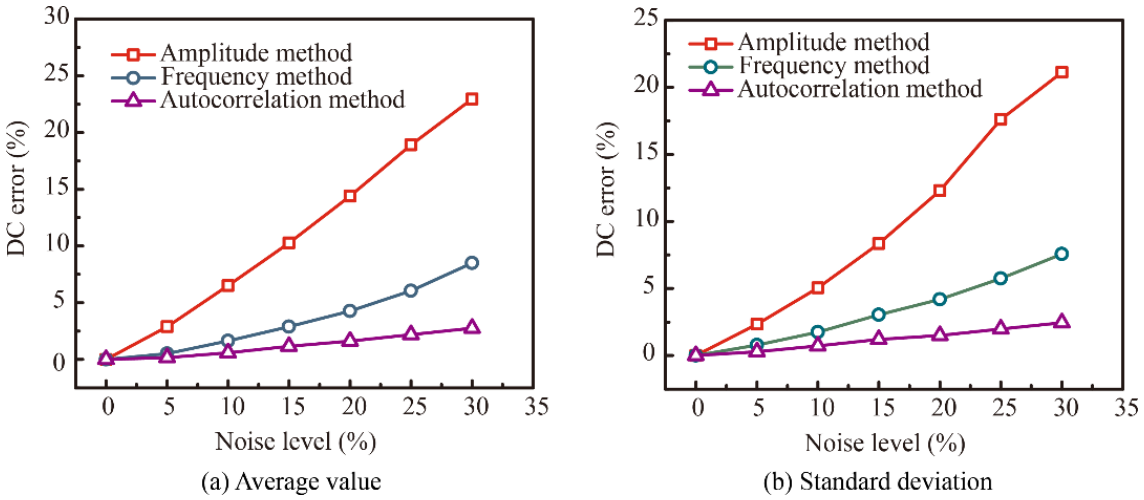

Figure 7. The errors of the retrieved DC proportions for the inversion of shear cracks calculated by the three methods.

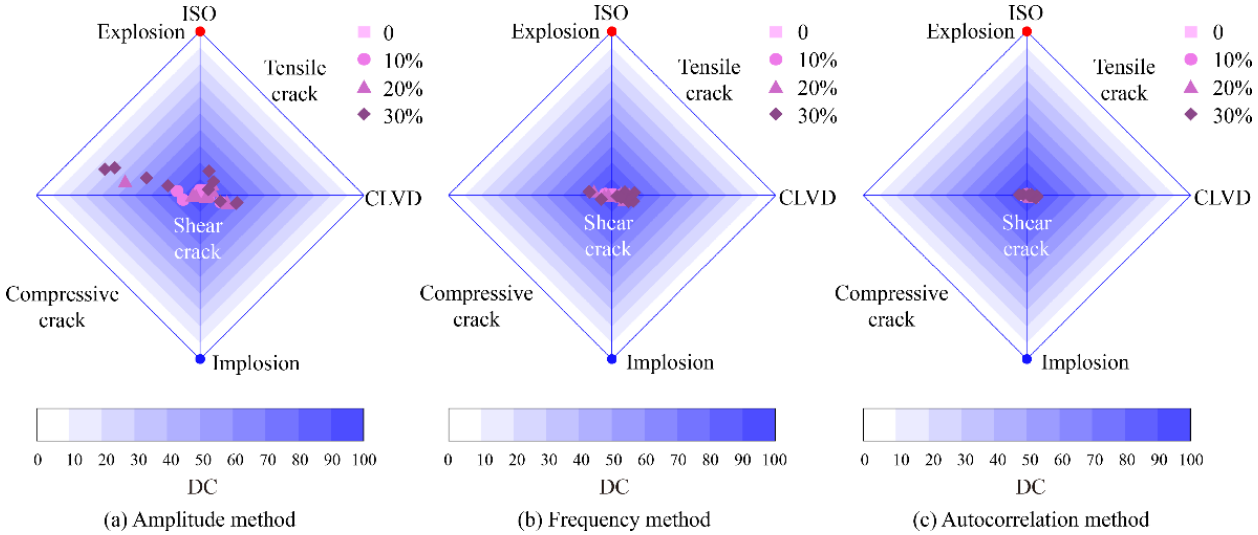

Figure 8. The source-type plots of the inversion results for shear cracks calculated by the three methods.

As shown in Figures 7 and 8, for shear cracks, the inversion errors of the DC proportions retrieved by the autocorrelation method are smaller than those of the amplitude and frequency methods. In addition, for the source-type plots, the results obtained by the

autocorrelation method are more concentrated and closer to the true values than those of the other two methods.

In Figures 5 and 7, an unusual phenomenon can be observed in which the standard deviation is of the same order of magnitude as the mean. This phenomenon can also be observed in some other references [23,26,37]. At present, the mechanism of this phenomenon is still unclear and needs further study.

Theoretically, any cracks can be a combination of pure tensile and shear cracks. Consequently, the feasibility of the inversion method based on the new correlation function of raw waveforms to any cracks can be proven by the above synthetic tests.

4. Discussion

According to the synthetic tests in Section 3, the performance of the inversion based on the new correlation function has been validated, and information on the noise or signal spectra is not required by the inversion process. However, according to the theoretical analysis in Section 2, two parameters may have an influence on the inversion accuracy and need further analysis. The parameters are the time shifts between correlation functions and signals and the difference in spectra between signals and noise. In this section, the effect of those two parameters on inversion accuracy is analyzed, and the applicative conditions of the new methodology are provided.

4.1. Time Shift

According to the theoretical analysis in Section 2.3, the best inversion accuracy can be achieved when the time shifts between correlation functions and signals are zero (as shown in Figure 9a). Although accurate source locations are helpful for extracting the slice of signals for calculation, noise contamination is inevitable. In this circumstance, the arriving and end signals are submerged in noise, and the first motions of waveforms cannot be picked precisely. Then, the time shifts between correlation functions and signals (as shown in Figure 9b) cannot be avoided, and the inversion accuracy is influenced. In this section, the influence of time shifts on inversion accuracy is analyzed. It should be noted that the time shift is different from the time delay in Equation (9). The time delay is the difference between the arrival time of the first motions and is caused by different source–sensor distances. The time shift is the picking error of the first motions and is caused by noise. The time delay does not cause inversion errors, but the time shift does.

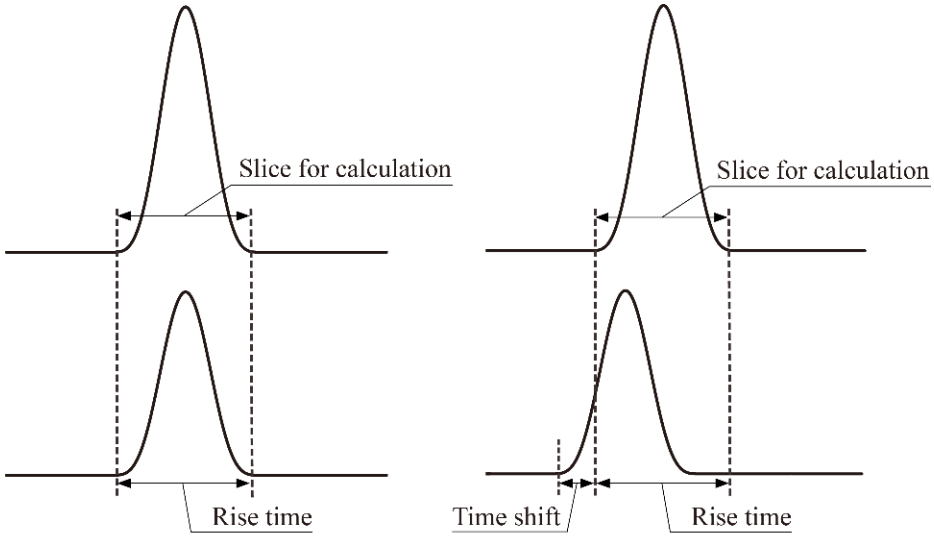

(a) Two waveforms without time shift (b) Two waveforms with time shift

Figure 9. Time shifts between correlation functions of raw waveforms and signals.

For generality, a new parameter of phase differences is defined as the ratio between time shifts and rise times.

The inversion results for various phase differences are plotted in Figure 10.

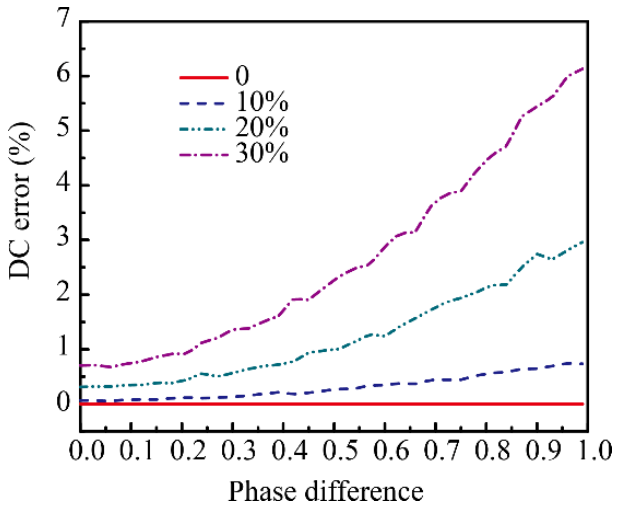

Figure 10. Inversion results for phase differences between correlation functions of raw waveforms and signals. For generality, the phase differences are defined as the ratios between time shifts and rise times. Line types represent four noise levels defined as the ratios between noise and signal amplitudes.

As shown in Figure 10, the inversion errors increase with the increase in the phase difference. If the effective slice of correlation functions cannot be picked precisely, the frequency spectrum of the slice (correlation function) is different from those of signals, and then the correlation calculation cannot efficiently amplify signals and suppress the effect of noise. Specifically, $C(\tau, u_s^1(t), u_s^2(t))$ in Equation (13) decreases and the correlation coefficient is more dependent on $C(\tau, u_n^1(t), u_s^2(t))$, which is related to noise. Then, the inversion results calculated by the correlation coefficient are inaccurate. Consequently, picking the first motions precisely is significant for the correlation calculation, and a time shift of 0 is recommended.

For engineering applications, a time shift of 0 is difficult to achieve, because the recorded signals are always contaminated by noise. Then, the inversion errors generated by the time shift are inevitable. However, according to Figure 10, the maximum inversion error is less than 7%, which is acceptable for most engineering applications. Thus, although a time shift of 0 can hardly be obtained, the new methodology can still provide the inversion results of acceptable accuracy.

4.2. Spectrum Difference

According to the theoretical analysis in Section 2.3, the spectra of signals are supposed to be different from that of noise. For engineering applications, the difference in spectra between the signals and noise is dependent on real conditions and may not be measurable for de-noising. Consequently, in this section, the dependence of the inversion accuracy on the spectrum difference between signals and noise is analyzed.

To quantify the spectrum difference, random white noise is replaced by sinusoidal noise to be added to the AE waveforms, and the frequency of noise is denoted as f_n. AE signals are pulse-like functions with broad spectra, thus the dominant frequency f_s (=$1/T_r$) is used for quantifying the spectra of AE signals. For generality, we define $\lg(f_n/f_s)$ to quantify the spectrum difference between signals and noise. The inversion errors of DC proportions for different $\lg(f_n/f_s)$ are plotted in Figure 11.

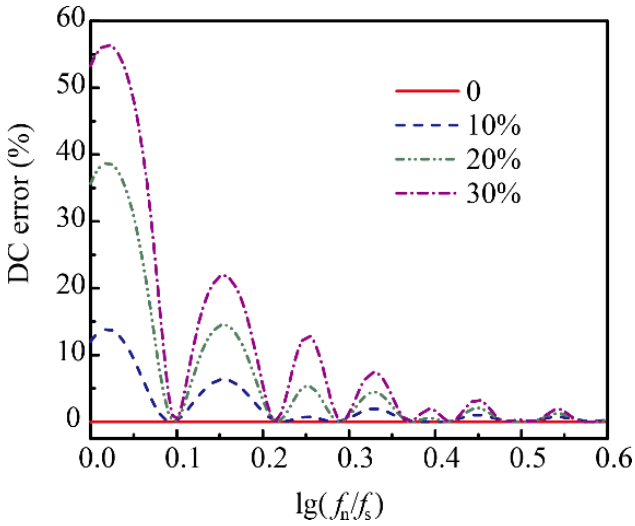

Figure 11. Inversion errors of DC proportions for the spectrum differences between signals and noise. f_n is the frequency of sinusoidal noise and f_s is the dominant frequency of signals. Line types represent the results of four noise levels.

As shown in Figure 11, when the spectrum difference is small, the inversion errors are significant, which indicates that the correlation calculation based on the correlation function of raw waveforms cannot filter out noise efficiently. When the spectrum difference between signals and noise is large enough ($\lg(f_n/f_s) > 0.5$ or $f_n/f_s > 3.2$), the inversion errors are approximately zero, which indicates that the noise is completely filtered out by the correlation calculation. Thus, the inversion method based on the new correlation function is effective when the frequency of noise is 3.2 times the dominant frequency of signals, and the optimal performance of de-noising can be achieved.

According to Figure 11, the inversion errors can be significant, when the spectrum of noise is similar to that of signals. However, for engineering applications, the spectrum of noise is commonly greater than that of signals by at least one order of magnitude. In this circumstance, the inversion error is less than 5%, which is acceptable. Consequently, the inversion method based on the new correlation function is suitable for most engineering applications.

5. Conclusions

In this study, a new correlation function of raw waveforms is proposed. The inversion method based on the new correlation function can improve the inversion accuracy with little additional computation consumption and does not require knowledge of the noise or signal spectra. This idea is based on the inherent similarity between the signals, which are generated by one source and recorded by different sensors. The spectrum of the new correlation function is identical to those of signals and the optimal performance of de-noising can be achieved by the correlation calculation, and then the accuracy of the moment tensors inverted by the correlation coefficients improves. Compared with other methods, the errors of the inversion method based on the new correlation function can be reduced up to 90%.

The new correlation function is suitable for all source types, such as tensile, shear, and mixed cracks. The performance of the new correlation function is influenced by the time shifts between correlation functions and signals and the spectrum difference between signals and noise. In normal circumstances, the inversion errors caused by those two factors are relatively small and the new correlation function can be applied to most cases.

Author Contributions: Conceptualization, Y.K. and M.L.; methodology, Y.K. and W.C.; software, Y.K.; validation, Y.K., N.L. and B.K.; writing—original draft preparation, Y.K.; supervision, W.C. and M.L.; funding acquisition, W.C. and N.L. All authors have read and agreed to the published version of the manuscript.

Funding: This research was funded by the Strategic Priority Research Program of the Chinese Academy of Sciences, grant number XDA22000000, and the National Natural Science Foundation of China, grant number 41804134.

Conflicts of Interest: The authors declare no conflict of interest.

References

1. Rokhlin, S.I.; Zoofan, B.; Kim, J.-Y. Microradiographic characterization of pitting corrosion damage and fatigue life. In *Review of Progress in Quantitative Nondestructive Evaluation*; Thompson, D.O., Chimenti, D.E., Eds.; Springer: Boston, MA, USA, 1999; Volume 18A–18B, pp. 1795–1804.
2. Bieber, J.A.; Tai, C.-C.; Moulder, J.C. Quantitative assessment of corrosion in aircraft structures using scanning pulsed eddy current. In *Review of Progress in Quantitative Nondestructive Evaluation*; Thompson, D.O., Chimenti, D.E., Eds.; Springer: Boston, MA, USA, 1998; Volume 17A, pp. 315–322.
3. Yan, Z.; Xiao, H.; Nagy, P.B. Ultrasonic detection of fatigue cracks by thermo-optical modulation. In *Review of Progress in Quantitative Nondestructive Evaluation*; Thompson, D.O., Chimenti, D.E., Eds.; Springer: Boston, MA, USA, 1999; Volume 18A–18B, pp. 1779–1786.
4. Grondel, S.; Delebarre, C.; Assaad, J.; Dupuis, J.-P.; Reithler, L. Fatigue crack monitoring of riveted aluminium strap joints by Lamb wave analysis and acoustic emission measurement techniques. *NDT E Int.* **2002**, *35*, 137–146. [CrossRef]
5. Joosse, P.A.; Blanch, M.J.; Dutton, A.G.; Kouroussis, D.A.; Philippidis, T.P.; Vionis, P.S. Acoustic Emission Monitoring of Small Wind Turbine Blades. *J. Sol. Energy Eng.* **2002**, *124*, 446–454. [CrossRef]
6. Yu, J.; Ziehl, P.; Zárate, B.; Caicedo, J. Prediction of fatigue crack growth in steel bridge components using acoustic emission. *J. Constr. Steel Res.* **2011**, *67*, 1254–1260. [CrossRef]
7. Martin, C.A.; Van Way, C.B.; Lockyer, A.J.; Kudva, J.N.; Ziola, S.M. Acoustic emission testing on an F/A-18 E/F titanium bulkhead. In *Smart Structures and Materials 1995: Smart Sensing, Processing, and Instrumentation*; SPIE: Bellingham, WA, USA, 1995.
8. Haile, M.A.; Bordick, N.E.; Riddick, J.C. Distributed acoustic emission sensing for large complex air structures. *Struct. Health Monit.* **2017**, *17*, 624–634. [CrossRef]
9. Han, C.; Liu, T.; Jin, Y.; Yang, G. Acoustic Emission Intelligent Identification for Initial Damage of the Engine based on Single Sensor. *Mech. Syst. Signal Process.* **2022**, *169*, 108789. [CrossRef]
10. Schijve, J. *Fatigue of Structures and Materials*; Springer: Dordrecht, The Netherlands, 2001.
11. Pook, L.; Greenan, A. Fatigue crack-growth characteristics of two magnesium alloys. *Eng. Fract. Mech.* **1973**, *5*, 935–946. [CrossRef]
12. Daiuto, R.; Hillberry, B. *The Effect of Thickness on Fatigue Crack Propagation in 7475-T731 Aluminum Alloy Sheet*; Purdue University: West Lafayette, IN, USA, 1984.
13. Zuidema, J.; Blaauw, H. The effect of shearlips on fatigue crack growths in A1-2024 sheet material. In Proceedings of the Third International Conference on Fatigue and Fatigue Thresholds, University of Virginia, Charlottesville, VA, USA, 28 June–3 July 1987.
14. Burridge, R.; Knopoff, L. Body force equivalents for seismic dislocations. *Bull. Seism. Soc. Am.* **1964**, *54*, 1875–1888. [CrossRef]
15. Aki, K.; Richards, P.G. *Quantitative Seismology*; University Science Books: Sausalito, CA, USA, 2002.
16. Vavryčuk, V.; Bohnhoff, M.; Jechumtálová, Z.; Kolář, P.; Šílený, J. Non-double-couple mechanisms of microearthquakes induced during the 2000 injection experiment at the KTB site, Germany: A result of tensile faulting or anisotropy of a rock? *Tectonophysics* **2008**, *456*, 74–93. [CrossRef]
17. Fojtíková, L.; Vavryčuk, V.; Cipciar, A.; Madarás, J. Focal mechanisms of micro-earthquakes in the Dobrá Voda seismoactive area in the Malé Karpaty Mts.(Little Carpathians), Slovakia. *Tectonophysics* **2010**, *492*, 213–229. [CrossRef]
18. Vavryčuk, V. Moment tensor decompositions revisited. *J. Seism.* **2014**, *19*, 231–252. [CrossRef]
19. Mustac, M.; Tkalcic, H. On the use of data noise as a site-specific weight parameter in a hierarchical bayesian moment tensor inversion: The case study of the Geysers and Long Valley Caldera earthquakes. *Bull. Seismol. Soc. Am.* **2017**, *107*, 1914–1922. [CrossRef]
20. Hallo, M.; Asano, K.; Gallovic, F. Bayesian inference and interpretation of centroid moment tensors of the 2016 Kumamoto earthquake sequence, Kyushu, Japan. *Earth Planets Space* **2017**, *69*, 134. [CrossRef]
21. Birialtsev, E.; Demidov, D.; Mokshin, E. Determination of moment tensor and location of microseismic events under conditions of highly correlated noise based on the maximum likelihood method. *Geophys. Prospect.* **2017**, *65*, 1510–1526. [CrossRef]
22. Jian, P.R.; Tseng, T.L.; Liang, W.T.; Huang, P.H. A new automatic full-waveform regional moment tensor inversion algorithm and its applications in the Taiwan area. *B. Seismol. Soc. Am.* **2018**, *108*, 573–587. [CrossRef]
23. Vavryčuk, V.; Kühn, D. Moment tensor inversion of waveforms: A two-step time-frequency approach. *Geophys. J. Int.* **2012**, *190*, 1761–1776. [CrossRef]
24. Nakano, M.; Kumagai, H.; Inoue, H. Waveform inversion in the frequency domain for the simultaneous determination of earthquake source mechanism and moment function. *Geophys. J. Int.* **2008**, *173*, 1000–1011. [CrossRef]

25. Cesca, S.; Buforn, E.; Dahm, T. Amplitude spectra moment tensor inversion of shallow earthquakes in Spain. *Geophys. J. Int.* **2006**, *166*, 839–854. [CrossRef]
26. Kong, Y.; Li, M.; Chen, W.; Liu, N.; Kang, B. A moment tensor inversion approach based on the correlation between defined functions and waveforms. *Phys. Earth Planet. Inter.* **2021**, *312*, 106674. [CrossRef]
27. Eyre, T.S.; van der Baan, M. The reliability of microseismic moment-tensor solutions: Surface versus borehole monitoring. *Geophysics* **2017**, *82*, KS113–KS125.
28. Grosse, C.U.; Ohtsu, M. *Acoustic Emission Testing*; Springer: Berlin/Heidelberg, Germany, 2008.
29. Kong, Y.; Li, M.; Chen, W.; Liu, N.; Kang, B. Moment-tensor inversion and decomposition for cracks in thin plates. *Chin. J. Aeronaut.* **2020**, *34*, 352–359. [CrossRef]
30. Wang, X.; Cai, J.; Zhou, Z. A Lamb wave signal reconstruction method for high-resolution damage imaging. *Chin. J. Aeronaut.* **2019**, *32*, 1087–1099. [CrossRef]
31. Liu, M.; Wang, Q.; Zhang, Q.; Long, R.; Cui, F.; Su, Z. Hypervelocity impact induced shock acoustic emission waves for quantitative damage evaluation using in situ miniaturized piezoelectric sensor network. *Chin. J. Aeronaut.* **2019**, *32*, 1059–1070. [CrossRef]
32. Jiao, R.; He, X.; Li, Y. Individual aircraft life monitoring: An engineering approach for fatigue damage evaluation. *Chin. J. Aeronaut.* **2018**, *31*, 727–739. [CrossRef]
33. Ohtsu, M. Source inversion of acoustic emission waveform. *Doboku Gakkai Ronbunshu* **1988**, *1988*, 71–79. [CrossRef]
34. Cai, M.; Kaiser, P.; Morioka, H.; Minami, M.; Maejima, T.; Tasaka, Y.; Kurose, H. FLAC/PFC coupled numerical simulation of AE in large-scale underground excavations. *Int. J. Rock Mech. Min. Sci.* **2006**, *44*, 550–564. [CrossRef]
35. Wang, X.C. *Finite Element Method*; Tsinghua University Press: Beijing, China, 2003.
36. Petružálek, M.; Jechumtálová, Z.; Kolář, P.; Adamová, P.; Svitek, T.; Šílený, J.; Lokajíček, T. Acoustic Emission in a Laboratory: Mechanism of Microearthquakes Using Alternative Source Models. *J. Geophys. Res. Solid Earth* **2018**, *123*, 4965–4982. [CrossRef]
37. Vavryčuk, V.; Adamová, P.; Doubravová, J.; Jakoubková, H. Moment Tensor Inversion Based on the Principal Component Analysis of Waveforms: Method and Application to Microearthquakes in West Bohemia, Czech Republic. *Seism. Res. Lett.* **2017**, *88*, 1303–1315. [CrossRef]